IEEE Access
Multidisciplinary | Rapid Review | Open Access Journal

Received August 12, 2020, accepted August 24, 2020, date of publication August 31, 2020, date of current version September 29, 2020.

Digital Object Identifier 10.1109/ACCESS.2020.3020543

Location-Aware Transmission for Two-Cell Wireless Networks With Caching

BIN JIANG[1], (Member, IEEE), FU-CHUN ZHENG[2], (Senior Member, IEEE), TONG PENG[3], ALISTER G. BURR[4], (Senior Member, IEEE), AND MIKE FITCH[5], (Member, IEEE)

[1]National Mobile Communications Research Laboratory, Southeast University, Nanjing 210096, China
[2]School of Electronic and Information Engineering, Harbin Institute of Technology (Shenzhen), Shenzhen 518055, China
[3]Department of Informatics Centre for Telecommunications Research, King's College London, London WC2R 2LS, U.K.
[4]Department of Electronic Engineering, University of York, York YO10 5DD, U.K.
[5]5G Innovation Centre, University of Surrey, Guildford GU2 7XH, U.K.

Corresponding author: Bin Jiang (bjiang@seu.edu.cn)

This work was supported in part by the U.K., Engineering and Physical Sciences Research Council under Grant EP/K040685/2, in part by the Shenzhen Science and Technology Program under Grant KQTD20190929172545139 and Grant JCYJ20180306171815699, and in part by the National Natural Science Foundation of China under Grant 61761136016 and Grant 61631018.

ABSTRACT A novel downlink transmission selection scheme based on the locations of users for network coded cache-enabled, Multiple-Input Multiple-Output (MIMO) systems is proposed in this paper. Caches are available at both base stations (BSs) and mobile terminals (MTs) and network coding is employed in order to reduce power consumption. We compare the analysis of the proposed scheme with a simple direct transmission scheme in terms of achievable sum rate and outage probability. It is shown that the proposed scheme is preferred for high transmit signal-to-noise ratio (SNR) and/or high cross-link channel gain ratio scenarios, while the simple direct transmission scheme is better for low SNR and/or low cross-link channel gain ratio. Motivated by this analytical results, we present a selection algorithm for location-aware transmission scheme for two-cell networks. Numerical results confirm our theoretical analysis.

INDEX TERMS Wireless caching, achievable sum rate, outage probability.

I. INTRODUCTION

Caching at the edge of mobile networks (e.g., at base stations (BSs), access points (APs), or mobile terminals (MTs)) is a promising key technology for 5G and beyond wireless networks [1]. The benefits of caching popular content in the BSs or APs, such as backhaul load relief, low access latency and lower energy consumption, as well as creating more cooperative MIMO opportunities, have been studied in, e.g., [2]–[10]. The authors in [11] have proposed a novel coded caching scheme in which both local and global caching gains can be achieved by designing a particular pattern in cache placement at the receivers and exploiting coding in delivery. A cache-aided interference management (CAIM) scheme for general networks with caches at both transmitters and receivers was discussed in [12]. The authors have designed a scheme which loads the caches judiciously in order to maximize the opportunity not only for zero-forcing the outgoing interference from the transmitters but also for interference cancellation at the receivers due to the cached content at the receivers. In [13], the comparison between different caching strategies has been addressed.

Inspired by [12], we in this paper first design a network coded caching scheme (''Scheme I''). The popular contents are divided into different files and cached at BSs and MTs separately. When two MTs require the same or different contents, network coding is implemented between files at the same BS before transmission. The MTs will recover the desired content by using the original cached files and the network coded files received from different BSs. Our scheme differs from the work in [12] in that network coded files are transmitted in different time slots in order to reduce the energy consumption.

We then compare the proposed scheme with an alternative approach (''Scheme II'') which to cache the popular contents at the BSs only (i.e., no need for MT caching). In this paper, we analyze and compare these two different schemes in terms of sum rate and outage probability and then propose a caching scheme selection algorithm based on the MT location information (or channel conditions).

The rest of the paper is organized as follows. In Section 2, an introduction to the system definition and the novel

The associate editor coordinating the review of this manuscript and approving it for publication was Zheng Chang.

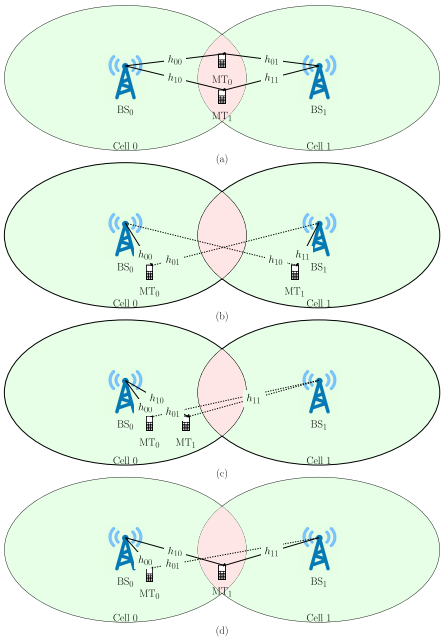

FIGURE 1. The system model: (a) Users are located at the cell edge. (b) Users are located near the different cell centers. (c) Users are located near the same cell center. (d) Users are located at the cell edge and near the cell center.

caching scheme will be presented. Section 3 will include the sum rate and outage probability analysis. In Section 4, an optimal caching methods selection algorithm will be proposed. Numerical results and discussion will be presented in Section 5, followed by the conclusions in Section 6.

II. SYSTEM MODEL

In this section, we introduce the downlink system model which involves 2 MTs and 2 BSs. Please note that the proposed cashing scheme can be extended to a larger network with multiple MTs and BSs [11], [12]. The focus of this paper is to evaluate the schemes in the simplest scenario applicable. Different scenarios are considered according to the locations of two MTs. A detailed channel model is derived followed by the introduction of two cache and delivery schemes.

A. THE CHANNEL MODEL

We consider the downlink of a cluster of two cooperating BSs and two MTs as shown in Fig. 1. The channel from the j^{th} BS to the i^{th} MT is modeled in the following form

$$h_{ij} = r_{ij}^{-\alpha/2} g_{ij}, \tag{1}$$

where $i, j \in \{0, 1\}$, $g_{ij} \sim \mathcal{CN}(0, 1)$ is a complex normally distributed random variable, $\alpha \geq 2$ denotes the path-loss exponent, and r_{ij} is the distance between the j^{th} BS and the i^{th} MT.

In Fig. 1, four cases of the downlink scenario based on the locations of the two MTs are illustrated. In Case (a), two MTs are located in the overlapped edge area of two cells, while one MT located in the overlapped edge area of two cells while another is near a cell center in Case (d). In Cases (b) and (c), none of the MTs are located in the overlapped cell edge area. The MTs are located near the centers of different cells in Case (b), and in Case (c), both MTs are located near the center of the same cell. In order to obtain explicit expressions and clear boundaries between the different cases, we define three parameters ω, κ_0 and κ_1, given by

$$\omega = (r_{00}/r_{11})^{\alpha}, \quad \kappa_0 = (r_{00}/r_{01})^{\alpha}, \quad \kappa_1 = (r_{11}/r_{10})^{\alpha}. \tag{2}$$

The above three parameters are the ratios of the mean cross-link channel gains, which characterize the balances of the cross-links. Without loss of generality, we set cell 0 in Fig. 1 as the reference, and thus the values of ω and κ_0 are between 0 and 1. The expressions for different cases are given in Table 1. It is worth noting that Case (a) is a special case of Cases (b), (c) and (d) in which $\kappa = 1, \omega = 1$ and $\omega = \kappa_0 = 1$, respectively. Under such a setup and assuming no channel state information (CSI) at the transmitter (i.e., BSs), two transmission schemes can be employed as described below.

TABLE 1. Parameters based on Users' Locations.

Case	Relation of r_{ij}	Relation of ω and κ_i
(a)	$r_{00} \approx r_{11} \approx r_{01} \approx r_{10}$	$\omega \approx 1,\ \kappa_0 \approx \kappa_1 \approx 1$
(b)	$r_{00} \approx r_{11},\ r_{01} \approx r_{10}$	$\omega \approx 1,\ \kappa_0 \approx \kappa_1 \approx \kappa$
(c)	$r_{00} \approx r_{10},\ r_{11} \approx r_{01}$	$\kappa_0 \approx \omega,\ \kappa_1 \approx \omega^{-1}$
(d)	$r_{10} \approx r_{11}$	$\kappa_1 \approx 1$

B. SCHEME I: CACHING AT BOTH BSs AND MTs

In Scheme I, as in [12], both the transmitters and receivers are equipped with caches. We define file A and B as two files stored in the library. Each BS and MT can cache at most a fraction μ_T and μ_R of the library content respectively, where $\mu_T, \mu_R \in [0, 1]$ is defined as the fractional cache size. For Scheme I, the BS and MT cache sizes are $\mu_T = 0.5$ and $\mu_R = 0.5$, respectively. In the prefetching phase, each file in the library is divided into 4 disjoint subfiles with the same size and then stored at the caches of the BSs and MTs. For example, file A is divided into $A_{0,0}, A_{0,1}, A_{1,0}, A_{1,1}$, where $A_{j,i}$ is stored at both the j^{th} BS and the i^{th} MT [12], $i, j \in \{0, 1\}$ (see Fig. 2(a)). File B is partitioned and stored in the same way.

Without loss of generality, we assume that MT_0 and MT_1 requests file A and B, respectively. Then the delivery phase is split into two time slots and in each delivery slot, one BS broadcasts a network coded signal while the other BS keeps silent. One example is shown in Fig. 2(b). In the first time slot, BS_0 transmits the content $A_{0,1} \oplus B_{0,0}$ and BS_1 keeps silent, where $\oplus$ stands the bit-wise XOR operation. In the second slot, BS_0 delivers the content $A_{1,1} \oplus B_{1,0}$ and BS_0 keeps silent. Other cases work in a similar fashion. The delivery scheme in [12] is illustrated in Fig. 2(c) where both BSs transmit contents at both time slots.

Let $x_j^{(k)}$ denote the transmitted signal from the j^{th} BS at the k^{th} time slot, then the received signal at the i^{th} MT in the k^{th}

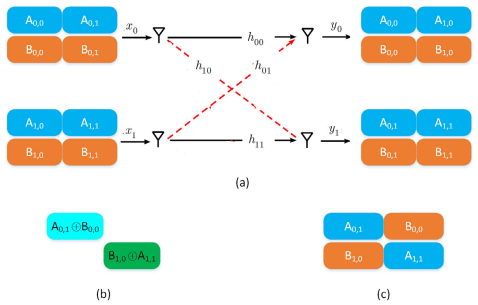

FIGURE 2. Caching and delivering strategy of Scheme I: (a) Coded caching at both BSs and MTs. (b) Proposed delivering scheme. (c) CAIM-based delivering scheme [12].

time slot can be expressed as

$$y_i^{(k)} = h_{ij}x_j^{(k)} + h_{ij'}x_{j'}^{(k)} + z_i^{(k)}, \quad j' \neq j, \tag{3}$$

where $z_i^{(k)}$ is the additive white Gaussian noise (AWGN) with independent real and imaginary parts of equal variance $N_0/2$.

In (3), different BSs transmit a network coded signal of different subfiles in different time slots, which indicates that $x_{j'}^{(k)} = 0$ when $x_j^{(k)} \neq 0$. This is very different from the scheme proposed in [12], where $x_j^{(k)}$ and $x_{j'}^{(k)}$ are non-zero and designed by a precoding algorithm, and $x_{j'}^{(k)}$ can be eliminated at the MTs. The non-zero symbol $x_j^{(k)}$ in the proposed scheme is obtained by simple XOR of the subfiles, and the desired subfile for different MTs can be recovered by using the cached subfiles. Another significant difference compared with the algorithm in [12] (see Fig. 2(c) for example) is that in the proposed scheme, one BS keeps silent while the other BS is transmitting, which means that the energy consumption of the proposed delivery scheme is half of that of the scheme in [12].

The instantaneous received signal-to-noise ratio (SNR) of the i^{th} BS at the k^{th} time slot can be expressed as

$$\gamma_{ij} = |h_{ij}|^2 E_s/N_0, \tag{4}$$

where E_s denotes the average energy per symbol of the non-zero transmitted signal. The average value of γ_{ij} is given by

$$\bar{\gamma}_{ij} = \mathsf{E}\{\gamma_{ij}\} = r_{ij}^{-\alpha} E_s/N_0. \tag{5}$$

By substituting (2) into (5), we have

$$\bar{\gamma}_{ij} = \begin{cases} \omega^i \gamma_0, & i = j, \\ \kappa_i \omega^i \gamma_0, & i \neq j, \end{cases} \tag{6}$$

where $\gamma_0 \triangleq r_{00}^{-\alpha} E_s/N_0$. Following [14], the normalized SNR is defined as $\rho_{ij} = \gamma_{ij}/\bar{\gamma}_{ij} = |g_{ij}|^2$. Since $g_{ij} \sim \mathcal{CN}(0, 1)$, the probability density function (PDF) of ρ_{ij} is given by

$$f_{ij}(x) = e^{-x}, \quad x \geq 0. \tag{7}$$

C. SCHEME II: CACHING AT BSs

In Scheme II, only BSs are equipped with caches. An MT is only served by its nearest BS, and each BS has cached all the files, (i.e., the BS and MT cache sizes are $\mu_T = 1$ and $\mu_R = 0$, respectively), which means that there is no cooperation between the BSs. With this assumption, the signal from the non-nearest BS will be treated as unknown interference [15]. We assume that the i^{th} MT is served only by the i^{th} BS. Then, the expression of the i^{th} MT's received signal is the same as in (3) except that x_j and x_j' are both non-zero. The instantaneous received signal-to-interference-plus-noise ratio (SINR) for the i^{th} MT is given by

$$\gamma_i = \frac{r_{ii}^{-\alpha}|g_{ii}|^2 E_s}{r_{ij}^{-\alpha}|g_{ij}|^2 E_s + N_0} = \frac{\omega^i \gamma_0 |g_{ii}|^2}{\mu_i |g_{ij}|^2 + 1}, \quad j \neq i. \tag{8}$$

where $\mu_i \triangleq \omega^i \kappa_i \gamma_0$. Similarly, the normalized SINR is defined as $\beta_i = \gamma_i/\bar{\gamma}_i$, where $\bar{\gamma}_i$ is the mean value of γ_i. The PDF of β_i can be derived as

$$q_i(x) = \frac{1+\mu_i+\psi(\mu_i)x}{(1+\psi(\mu_i)x)^2} \frac{\psi(\mu_i)}{\mu_i} \exp\left(-\frac{\psi(\mu_i)}{\mu_i}x\right), \quad x > 0, \tag{9}$$

where

$$\psi(x) \triangleq e^{1/x} E_1(1/x), \tag{10}$$

and $E_1(x)$ is the exponential integral function [16].

Proof: Please refer to Appendix A. ■

It is worth noting that the cache and transmission strategies of Schemes I and II do not need channel state information at the transmitters (CSIT). The system performance can be improved by utilizing the instantaneous CSIT at very short time scales. However, in this work, the transceiver strategy is designed by using the location information of users at longer time scales [17], [18].

III. PERFORMANCE ANALYSIS

In this section, the achievable average sum rate and outage probability of Scheme I and II are given. The four cases illustrated in Fig. 1 have been considered in both schemes in order to address the effect of different locations of the MTs to the schemes.

A. ACHIEVABLE SUM RATE ANALYSIS

For Scheme I, the average achievable sum rate is defined as

$$R_1 = \frac{1}{4}\sum_{i=0}^{1}\sum_{j=0}^{1}\int_0^\infty f_{ij}(x)\ln(1+x\bar{\gamma}_{ij})dx, \tag{11}$$

where $f_{ij}(x)$ is the PDF of ρ_{ij} and $\bar{\gamma}_{ij}$ is the mean value of γ_{ij}. Substituting (5) and (7) into (11) and using the equality $\int_0^\infty \exp(-x)\ln(1+ax)dx = \psi(a)$ [16, 4.337.2] yields

$$R_1 = \frac{\psi(\gamma_0) + \psi(\omega\gamma_0) + \psi(\kappa_0\gamma_0) + \psi(\kappa_1\omega\gamma_0)}{4}. \tag{12}$$

For Scheme II, the average achievable sum rate is defined as

$$R_2 = \frac{1}{2}\sum_{i=0}^{1}\int_0^\infty q_i(x)\ln(1+x\bar{\gamma}_i)dx, \tag{13}$$

where $q_i(x)$ is the PDF of β_i and $\bar{\gamma}_i$ is the mean value of γ_i. R_2 can be expressed as

$$R_2 = \begin{cases} \frac{1}{2}\sum_i \frac{\psi(\omega^i\gamma_0) - \psi(\kappa_i\omega^i\gamma_0)}{\omega^i - \kappa_i\omega^i}, & \kappa_i \neq 1, \\ \frac{1}{2}\left(1 - \frac{\psi(\omega^j\gamma_0)}{\omega^j\gamma_0} + \frac{\psi(\omega^i\gamma_0) - \psi(\kappa_i\omega^i\gamma_0)}{\omega^i - \kappa_i\omega^i}\right) & \begin{matrix}\kappa_i \neq 1, \\ \kappa_j = 1, \\ i \neq j,\end{matrix} \\ \frac{1}{2}\sum_i \left(1 - \frac{\psi(\omega^i\gamma_0)}{\omega^i\gamma_0}\right), & \kappa_i = 1. \end{cases} \tag{14}$$

Proof: Please refer to Appendix B. ■

The function $\psi(x)$ is important to the average achievable sum rates of Scheme I and Scheme II derived in (12) and (14): it can be defined as the ergodic capacity of Rayleigh fading channels [19], [20]. $\psi(x)$ includes the non-elementary function $E_1(x)$, which makes it difficult to obtain much insight about the sum-rate. Estimations of $\psi(x)$ based on series expansions can be found in [19], [20], while polynomial and rational approximations of $\psi(x)$ can be found in [21]. For further discussions, we need to investigate the monotonicity of $\psi(x)$ and its related functions, and the main results are summarized in the following lemma.

Lemma 1: The function $\psi(x)$ is monotonically increasing in x. For the following $\psi(x)$ related functions

$$\theta_1(x) = \frac{\psi(x)}{x}, \quad x > 0, \tag{15}$$

$$\theta_2(x) = \psi(x) + \frac{\psi(x)}{x} - 1, \quad x > 0, \tag{16}$$

$$\theta_3(x) = \psi(ax) - \psi(bx), \quad x > 0,\ a > 0,\ b > 0, \tag{17}$$

$$\theta_4(x) = \frac{\psi(b) - \psi(bx)}{1 - x}, \quad x > 0,\ x \neq 1,\ b > 0, \tag{18}$$

$\theta_1(x)$ and $\theta_4(x)$ are monotonically decreasing in x, $\theta_2(x)$ is monotonically increasing in x, and $\theta_3(x)$ is monotonically increasing and decreasing in x for $a > b$ and $a < b$, respectively.

Proof: Please refer to Appendix C. ■

With the general results of average achievable sum-rates for Scheme I and Scheme II as shown in (12) and (14), we give the sum-rate expressions for Cases (a) to (d) as follows.

Case (a): In this case, both ω and κ_i are assumed to be constants. By substituting $\omega = 1$ and $\kappa_0 = \kappa_1 = 1$ into (12) and (14), we have

$$R_1^{(a)} = \psi(\gamma_0), \tag{19}$$

$$R_2^{(a)} = 1 - \psi(\gamma_0)/\gamma_0. \tag{20}$$

According to the monotonicity of $\psi(x)$ and $\theta_1(x)$ established in Lemma 1, both $R_1^{(a)}$ and $R_2^{(a)}$ are monotonically increasing with respect to γ_0.

Case (b): In this case, we assume that the MTs' locations are symmetrical with respect to the cell edge. We also assume that $0 < \kappa < 1$. If $\kappa = 1$, Case (b) reduces to Case (a). By substituting $\omega = 1$ and $\kappa_0 = \kappa_1 = \kappa$ into (12) and (14), we have

$$R_1^{(b)} = \frac{\psi(\gamma_0) + \psi(\kappa\gamma_0)}{2}, \tag{21}$$

$$R_2^{(b)} = \frac{\psi(\gamma_0) - \psi(\kappa\gamma_0)}{1 - \kappa}. \tag{22}$$

According to the monotonicity of $\psi(x)$, $\theta_3(x)$ and $\theta_4(x)$ derived in Lemma 1, we conclude that $R_1^{(b)}$ is monotonically increasing in both γ_0 and κ, while $R_2^{(b)}$ is monotonically increasing in γ_0 and decreasing in κ.

Case (c): In this case, we assume $0 < \omega < 1$. If $\omega = 1$, it transforms to Case (a). Substituting $\kappa_0 = \omega$ and $\kappa_1 = \omega^{-1}$ into (12) and (14) yields

$$R_1^{(c)} = \frac{\psi(\gamma_0) + \psi(\omega\gamma_0)}{2}, \tag{23}$$

$$R_2^{(c)} = \frac{\psi(\gamma_0) - \psi(\omega\gamma_0)}{1 - \omega}. \tag{24}$$

Interestingly, the only difference between the sum-rate expression in Case (c) and that in Case (b) is the use of the parameters ω or κ.

Case (d): In this case, we assume $0 < \omega < 1$ and $0 < \kappa_0 < 1$. Case (a) is obtained if $\omega = \kappa_0 = 1$. Then by substituting $\kappa_1 = 1$ into (12) and (14) gives

$$R_1^{(d)} = \frac{\psi(\gamma_0) + 2\psi(\omega\gamma_0) + \psi(\kappa_0\gamma_0)}{4}, \tag{25}$$

$$R_2^{(d)} = \frac{1}{2} - \frac{\psi(\omega\gamma_0)}{2\omega\gamma_0} + \frac{\psi(\gamma_0) - \psi(\kappa_0\gamma_0)}{2(1 - \kappa_0)}. \tag{26}$$

According to Lemma 1, $R_1^{(d)}$ is monotonically increasing in γ_0, κ_0 and ω, while $R_2^{(d)}$ is monotonically increasing in both γ_0 and ω and decreasing in κ_0.

B. OUTAGE PROBABILITY ANALYSIS

The outage probability is another important performance indicator in order to evaluate communication over fading channels; it indicates the probability that the instantaneous SNR or SINR falls below a certain threshold γ_{th} [14], [22]. The average outage probabilities of Schemes I and II are given by

$$P_1 = \frac{1}{4}\sum_{i=0}^{1}\sum_{j=0}^{1}\int_0^{\frac{\gamma_{th}}{\bar{\gamma}_{ij}}} f_{ij}(x)dx$$

$$= 1 - \frac{1}{4}\sum_{i=0}^{1}\left(\exp\left(-\frac{\gamma_{th}}{\omega^i\gamma_0}\right) + \exp\left(-\frac{\gamma_{th}}{\kappa_i\omega^i\gamma_0}\right)\right). \tag{27}$$

$$P_2 = \frac{1}{2}\sum_{i=0}^{1}\int_0^{\frac{\gamma_{th}}{\bar{\gamma}_i}} q_i(x)dx$$

$$= 1 - \frac{1}{2}\sum_{i=0}^{1}\frac{1}{1 + \kappa_i\gamma_{th}}\exp\left(-\frac{\gamma_{th}}{\omega^i\gamma_0}\right). \tag{28}$$

In general, P_1 is monotonically decreasing in γ_0, κ_i and ω, while P_2 is monotonically decreasing in γ_0 and ω and increasing in κ_i. With Table 1, we can obtain the expressions of the outage probabilities for Cases (a)-(d). We omit here for brevity.

IV. LOCATION-AWARE DELIVERY SCHEME SELECTION ALGORITHM

Based on the analysis in the previous section, clearly, a key question is: which caching/transmission scheme should be used under which conditions? As such, this section will discuss the conditions under which Scheme I or II should be selected.

The caching/transmission scheme selection criteria are designed based on the comparison of sum rates and outage probabilities of Schemes I and II. It is worth pointing out that the conditions are determined by the user locations (r_{ij} or equivalently ω and κ_i, $i, j \in \{0, 1\}$) and the transmit SNR.

Proposition 1: According to the locations of MTs described in Cases (a) to (d), the conditions that Scheme I achieves a higher sum rate than Scheme II are given by

- $R_1^{(a)} > R_2^{(a)}$ for all $\gamma_0 > 0$.
- $R_1^{(b)} \geq R_2^{(b)}$ if and only if the condition that
$$(3-\kappa)\psi(\kappa\gamma_0) - (1+\kappa)\psi(\gamma_0) \geq 0 \tag{29}$$
is satisfied.
- $R_1^{(c)} \geq R_2^{(c)}$ if and only if the condition (29) (κ replaced by ω) is satisfied.
- $R_1^{(d)} \geq R_2^{(d)}$ if and only if the condition that
$$\frac{(3-\kappa_0)\psi(\kappa_0\gamma_0)-(1+\kappa_0)\psi(\gamma_0)}{1-\kappa_0} + 2\theta_2(\omega\gamma_0) \geq 0 \tag{30}$$
is satisfied, and $R_1^{(d)} > R_2^{(d)}$ if the condition (29) (κ replaced by κ_0) is satisfied.

Proof: For Case (a), the difference between $R_1^{(a)}$ and $R_2^{(a)}$ can be expressed as $\theta_2(\gamma_0)$. Since $\lim_{\gamma_0\to 0}\psi(\gamma_0) = 0$, $\lim_{\gamma_0\to 0}\psi(\gamma_0)/\gamma_0 = 1$, and $\theta_2(\gamma_0)$ is monotonically increasing in γ_0, we have $\theta_2(\gamma_0) > \theta_2(0) = 0$, i.e., $R_1^{(a)} > R_2^{(a)}$ for all $\gamma_0 > 0$. For Cases (b)-(d), the necessary and sufficient conditions are obtained by directly simplifying the corresponding inequality $R_1 \geq R_2$. The sufficient condition for Case (d) is obtained by using the fact that the term $\theta_2(\omega\gamma_0)$ in (30) is always grater than zero for all γ_0 and ω.

Special cases for Case (b): (i) If the value of γ_0 is large, then the condition (29) will always hold for all $\kappa > 0$, which means that Scheme I achieves higher sum rate than Scheme II when the SNR is high. (ii) If κ approaches 1, then the condition (29) will always hold, which means that Scheme I achieves higher sum rate than Scheme II when the cross-link channel gain is strong enough. (iii) If κ approaches 0, then the condition (29) will not hold, which means that Scheme II is preferred when the cross-link channel gain is weak. ■

The scheme selection criteria according to outage probability for Cases (a) to (d) are contained in the following proposition.

Proposition 2: Considering the locations of MTs in Section II-A, the conditions that Scheme I achieves lower outage probabilities than Scheme II in Cases (a) to (d) are given by

- $P_1^{(a)} < P_2^{(a)}$ for all $\gamma_0 > 0$.
- $P_1^{(b)} \leq P_2^{(b)}$ if and only if the condition that
$$\gamma_0 \geq \frac{(1-\kappa)\gamma_{th}}{\kappa\left(\ln(1+\kappa\gamma_{th}) - \ln(1-\kappa\gamma_{th})\right)} \tag{31}$$
is satisfied.
- $P_1^{(c)} < P_2^{(c)}$ for all $\gamma_0 > 0$ and $0 < \omega < 1$.
- $P_1^{(d)} \leq P_2^{(d)}$ if and only if the following condition
$$\frac{2\gamma_{th}}{1+\gamma_{th}} e^{-\frac{\gamma_{th}}{\omega\gamma_0}} + e^{-\frac{\gamma_{th}}{\kappa_0\gamma_0}} \geq \frac{1-\kappa_0\gamma_{th}}{1+\kappa_0\gamma_{th}} e^{-\frac{\gamma_{th}}{\gamma_0}} \tag{32}$$
is satisfied.

Proof: For Cases (a) and (c), by respectively substituting $\omega = \kappa_0 = \kappa_1 = 1$ and $\omega = \kappa_0 = \kappa_1^{-1}$ into (27) and (28), we have

$$P_1^{(a)} - P_2^{(a)} = -\frac{\gamma_{th}}{1+\gamma_{th}} e^{-\frac{\gamma_{th}}{\gamma_0}}, \tag{33}$$

$$P_1^{(c)} - P_2^{(c)} = -\frac{1}{2}\left(\frac{\gamma_{th}}{1+\gamma_{th}} e^{-\frac{\gamma_{th}}{\gamma_0}} + \frac{\gamma_{th}}{\omega+\gamma_{th}} e^{-\frac{\gamma_{th}}{\omega\gamma_0}}\right). \tag{34}$$

Thus, $P_1^{(a)} < P_2^{(a)}$ for all $\gamma_{th} > 0$ and $P_1^{(c)} < P_2^{(c)}$ for all $\gamma_{th} > 0$ and $\omega > 0$. For Cases (b) and (d), the necessary and sufficient conditions are obtained by simplifying the corresponding inequality $P_1 \leq P_2$. ■

Proposition 2 indicates that the outage probability of Scheme I is always lower than that of Scheme II for grouped users (Cases (a) and (c)), no matter where the group of users are located in a cell.

We now discuss some extreme cases for the condition as shown in (31). (i) The condition (31) will always hold if γ_0 approaches infinity, while it will not hold if γ_0 approaches zero. This property means that Scheme I and Scheme II should be selected to achieve the lower outage probability in high and low SNR regions, respectively. (ii) The condition (31) will always hold if κ approaches 1, while it will not hold if κ approaches 0. Hence, Scheme I should be selected for strong cross-links, while Scheme II should be selected for weak cross-links. (iii) For Case (d), if ω approaches 0, then the condition in (32) reduces to the condition in (31). In addition, (32) will always hold if ω approaches 1 and $\gamma_{th} \geq 1$.

V. NUMERICAL RESULTS

A. ACHIEVABLE SUM RATE

Fig. 3 shows the achievable sum rates for Case (b).[1] It is worth pointing out that Case (a) is a special case of Case (b) with $\kappa = 1$. Fig. 3(a) indicates the average sum rate as a function of γ_0 with different κ, while Fig. 3(b) shows the average sum rate as a function of κ with different γ_0. The curves with and without markers depict the Monte-Carlo and analytical results, respectively. Clearly, our theoretical analysis matches the numerical results very well. According to Fig. 3(a), there is a switching point of γ_0 for a given value of κ. For example, if $\kappa = -12$ dB, then the average sum rate of Scheme I will

[1] If we replace the parameter κ in Fig. 3 with ω, then this figure becomes the achievable sum rates for Case (c).

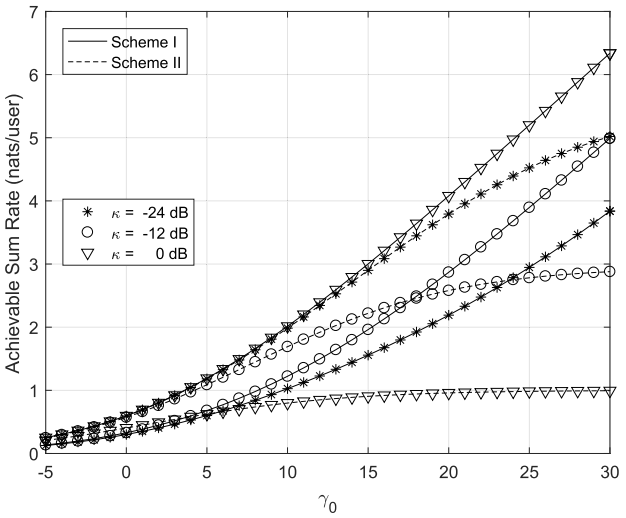

(a) Achievable sum rate versus γ_0 with different κ.

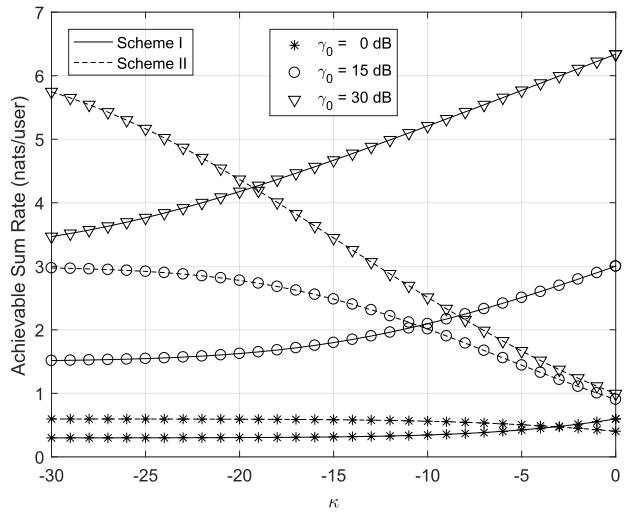

(b) Achievable sum rate versus κ with different γ_0.

FIGURE 3. Achievable sum rate for Case (b).

outperform that of Scheme II when $\gamma_0 \geq 18$ dB. Similarly, Fig. 3(b) illustrates a switching point of κ for a given value of γ_0. For example, if $\gamma_0 = 15$ dB, then the average sum rate of Scheme I will outperform that of Scheme II when $\kappa \geq -10$ dB.

Fig. 4 displays the achievable sum rates for Case (d) in terms of γ_0, κ_0 and ω. For each of these three figures, one of these variables changes over the whole range, while the remaining two variables take two typical and fixed values. From Fig. 4(a), we have the following observations: (i) Scheme I is always better than Scheme II when $\kappa_0 = 0$ dB. (ii) If $\kappa_0 = -10$ dB, then Scheme I will be better than Scheme II when $\gamma_0 > 1$ dB and $\gamma_0 > 11$dB for $\omega = 0$ dB and $\omega = -10$ dB, respectively. Fig. 4(b) shows that: (i) Scheme I is always better than Scheme II when $\gamma_0 = 30$ dB. (ii) If $\gamma_0 = 15$ dB, then Scheme I will be always better than Scheme II for $\omega = 0$ dB, and is conditionally better than Scheme II for $\omega = -10$ dB when $\kappa_0 > -14$ dB.

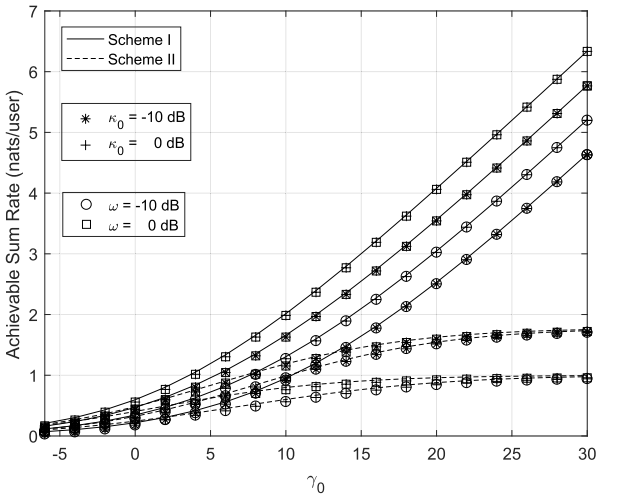

(a) Achievable sum rate versus γ_0 with different κ_0 and ω.

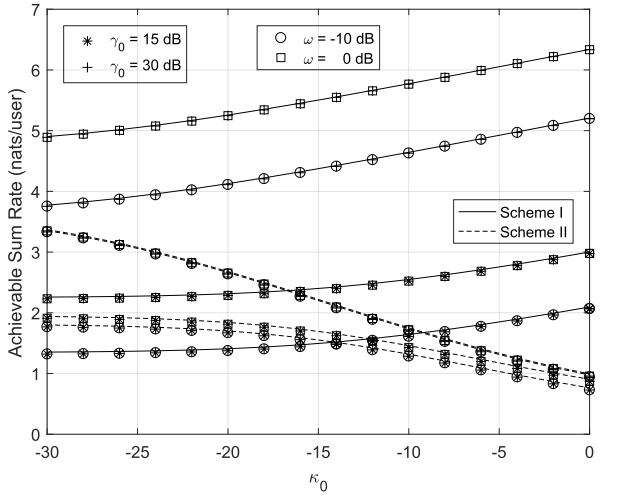

(b) Achievable sum rate versus κ_0 with different γ_0 and ω.

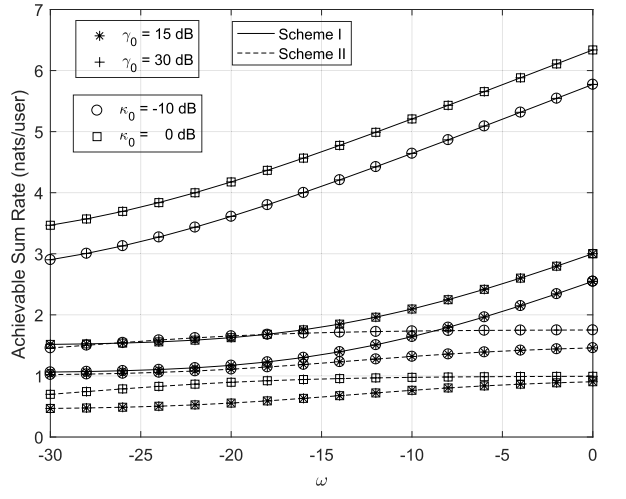

(c) Achievable sum rate versus ω with different γ_0 and κ_0.

FIGURE 4. Achievable sum rate for Case (d).

Fig. 4(c) indicates that Scheme I will always be better than Scheme II for all ω with the selected typical values of γ_0 and κ_0.

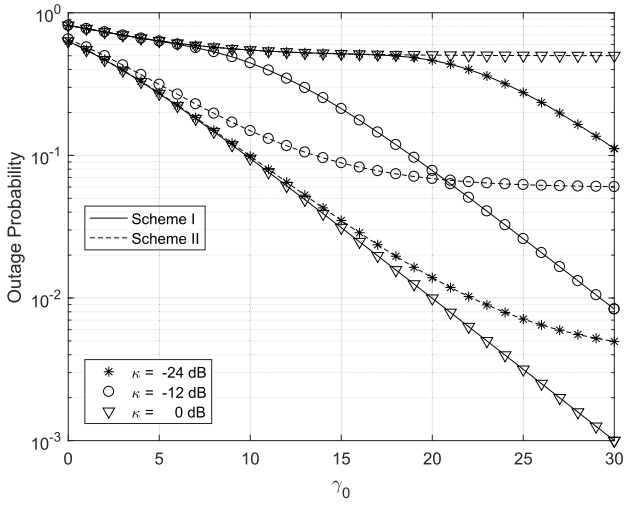

(a) Outage probability versus γ_0 with different κ.

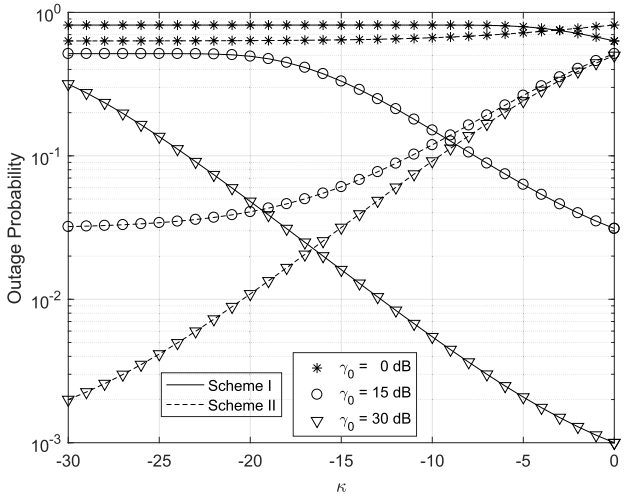

(b) Outage probability versus κ with different γ_0.

FIGURE 5. **Outage probability for Case (b).**

B. OUTAGE PROBABILITY

Fig. 5 shows the outage probabilities of Case (b).[2] The SNR threshold γ_{th} is set to 0 dB. We observe that: (i) Schemes I and II will be always better for all $\gamma_0 > 0$ when κ is big enough (e.g., 0 dB) and small enough (e.g., -24 dB), respectively. However, for moderate values of κ (e.g., -12 dB), there is a switching point ($\gamma_0 = 21$ dB) between Schemes I and II. (ii) If $\gamma_0 = 15$ dB, then Scheme I is better than Scheme II only when $\kappa > -9$ dB. (iii) The switching point of κ will decrease when the SNR γ_0 increases.

Fig. 6 shows the outage probabilities of Case (d) with respect to γ_0, κ_0 and ω. We observe from Fig. 6(a) that: (i) Scheme I is always better than Scheme II when the SNR γ_0 is high enough, or $\kappa_0 = 0$ dB or $\omega = 0$ dB. (ii) In case of $\kappa_0 = \omega = -10$ dB, the switching point of Scheme I and Scheme II is $\gamma_0 = 10$ dB. Fig. 6(b): (i) Scheme I is always better than Scheme II when the κ_0 is big enough, or $\gamma_0 = 30$ dB or $\omega = 0$ dB. (ii) In case of $\gamma_0 = 15$ dB and $\omega = -10$ dB, the switching point between Schemes I and II is $\kappa_0 = -16$ dB. Fig. 6(c): (i) Scheme I is always better

[2]For Cases (a) and (c), both the monotonicity and the optimality of Scheme I have been analytically discussed in Sec. III, so we omit their numerical results for brevity.

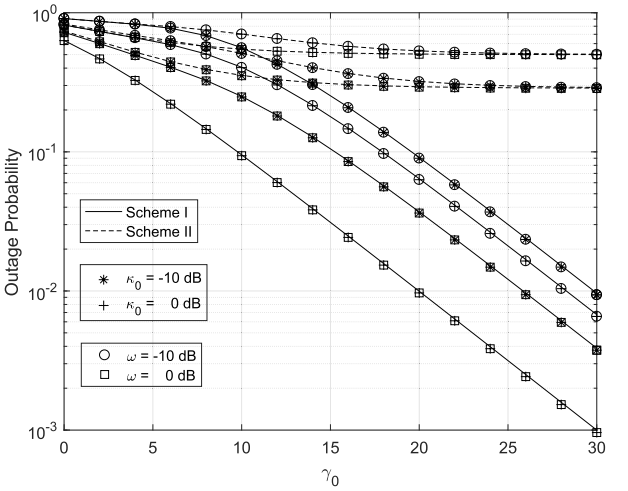

(a) Outage probability versus γ_0 with different κ_0 and ω.

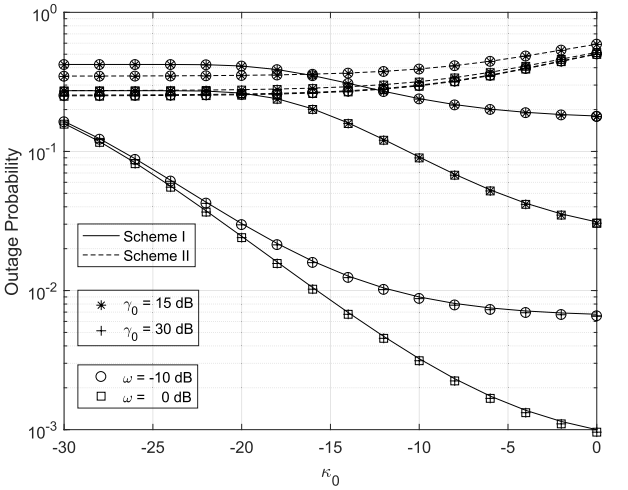

(b) Outage probability versus κ_0 with different γ_0 and ω.

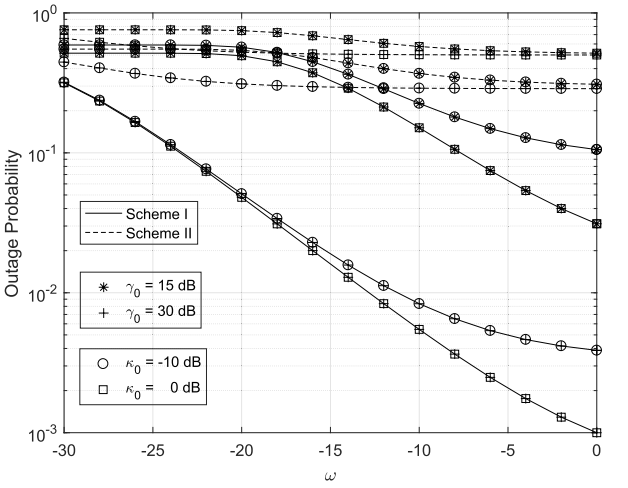

(c) Outage probability versus ω with different γ_0 and κ_0.

FIGURE 6. **Outage probability for Case (d).**

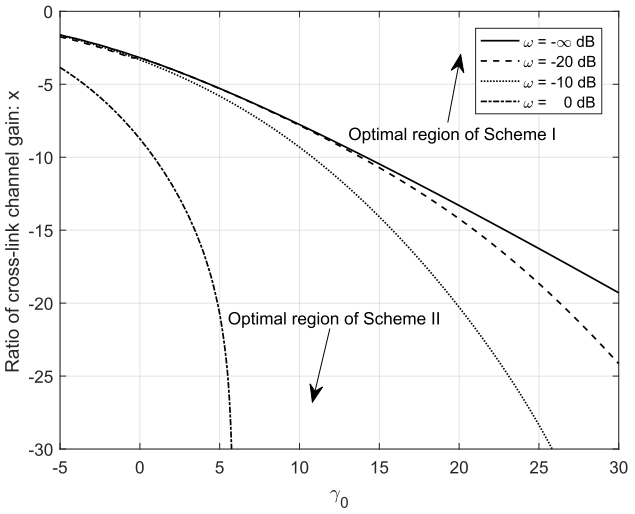

(a) Optimal regions based on achievable sum rate.

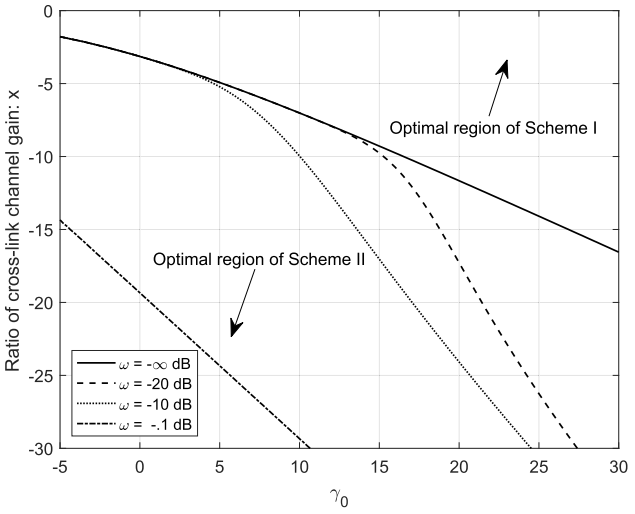

(b) Optimal regions based on outage probability.

FIGURE 7. Optimal regions of Schemes I and II.

than Scheme II when the ω is big enough, or $\gamma_0 = 30$ dB or $\kappa_0 = 0$ dB. (ii) In case of $\gamma_0 = 15$ dB and $\omega = -10$ dB, the switching point between Schemes I and II is $\omega = -18$ dB.

C. SWITCHING REGION BETWEEN SCHEMES I AND II

The switching regions between Schemes I and II based on achievable sum rate and outage probability are plotted in Fig. 7(a) and Fig. 7(b), respectively. The figures clearly mark out the regions where inequality in Proposition 1 or Proposition 2 is satisfied, meaning that Scheme I is the better strategy; while the region where the inequality is reversed implies that Scheme II is better. In both figures, the Y-axis variable x stands for the ratio of cross-link channel gain. By replacing x with κ, ω and κ_0, we obtain the results for Cases (b), (c) and (d), respectively. Note that the optimal strategy depends on both the average transmitted SNR γ_0 and the cross-link channel gain ratio x. In general, for high SNR and/or high cross channel gain ratio, the better strategy is Scheme I, while for low SNR and/or low cross channel gain ratio, Scheme II is the better strategy.

VI. CONCLUSION

We have proposed a novel network coded caching scheme for two-cell downlink networks. In order to investigate its performance, the achievable sum-rate and outage probability have been derived in closed-form. A comparison between the proposed scheme and a simple direct transmission scheme has also been conducted and a location-based cache/transmit scheme selection algorithm has been explored. The proposed selection scheme allows BSs to select cache and transmit scheme for different scenarios based on different locations of MTs in order to achieve higher sum rate or lower outage probability.

APPENDIX A
PDF OF THE NORMALIZED SINR β_i

We first derive the PDF of the instantaneous SINR for the i^{th} MT. From (8), we see that γ_i is a ratio of two independent random variables X_i and Y_i, both of which are the linear transform of chi-squared variables with 2 degrees of freedom, and their distributions are respectively given by

$$U_{X_i}(x) = \frac{1}{r_{ii}^{-\alpha}\gamma_0} \exp\left(-\frac{x}{r_{ii}^{-\alpha}\gamma_0}\right), \quad x > 0, \tag{35}$$

$$U_{Y_i}(y) = \frac{1}{r_{ij}^{-\alpha}\gamma_0} \exp\left(-\frac{y-1}{r_{ij}^{-\alpha}\gamma_0}\right), \quad y > 1. \tag{36}$$

Then, the ratio distribution can be obtained from integration of the following form [23]

$$U_{\gamma_i}(z) = \int_{-\infty}^{\infty} |y| U_{X_i}(yz) U_{Y_i}(y) dy. \tag{37}$$

By substituting (35) and (36) into (37), we have

$$U_{\gamma_i}(z) = \frac{1 + \omega^i \kappa_i \gamma_0 + \kappa_i z}{\omega^i \gamma_0 (1 + \kappa_i z)^2} \exp\left(-\frac{z}{\omega^i \gamma_0}\right). \tag{38}$$

The mean of the γ_i is

$$\bar{\gamma}_i \triangleq \int_0^{\infty} z U_{\gamma_i}(z) dz = \frac{\psi(\omega^i \kappa_i \gamma_0)}{\kappa_i}. \tag{39}$$

Thus, the PDF of normalized SINR β_i can be expressed as

$$q_i(x) = \bar{\gamma}_i U_{\gamma_i}(\bar{\gamma}_i x). \tag{40}$$

Substituting (38) and (39) into (40) yields (9). This completes the proof.

APPENDIX B
DERIVATION OF (14)

From (9), the integration of $q_i(x)$ can be written in the following closed-form

$$\int q_i(x) dx = -\frac{1}{1 + \psi(\mu_i) x} \exp\left(-\frac{\psi(\mu_i)}{\mu_i} x\right). \tag{41}$$

Let $y \triangleq \frac{\psi(\mu_i)}{\mu_i}x$, then the i^{th} summation term of (13) can be calculated as

$$R_{2,i} = \int_0^\infty \ln\left(1+\omega^i\gamma_0 y\right) d\left(-\frac{\exp(-y)}{1+\mu_i y}\right), \quad (42)$$

$$= \int_0^\infty \frac{\omega^i\gamma_0 \exp(-y)}{(1+\omega^i\gamma_0 y)(1+\kappa_i\omega^i\gamma_0 y)} dy. \quad (43)$$

The integration of (43) can be calculated by using the identities [16, 3.252.4] and [16, 3.353.3] for the conditions that $\kappa_i \neq 1$ and $\kappa_i = 1$, respectively, which yields (14). This completes the proof.

APPENDIX C
PROOF OF LEMMA 1

According to the definition of $\psi(x)$ as in (10), we have

$$\psi(1/x) = e^x E_1(x). \quad (44)$$

The right-hand side (RHS) of (44) is a well studied function in the literature [21], [24], [25]. By simple transformation of the inequalities of [21, 5.1.19, 5.1.20], we have the following upper and lower bounds of $\psi(x)$:

$$\frac{x}{1+x} < \psi(x) < x, \quad (45)$$

$$\frac{1}{2}\ln(1+2x) < \psi(x) < \ln(1+x). \quad (46)$$

With (46), we can easily obtain the limits of $\psi(x)$ and its related functions, as x approaches 0 or ∞. However, we omit the derived results here for brevity.

Now we begin to prove the monotonicity and convexity of $\psi(x)$, which is useful for proving the monotonicity of functions related to $\psi(x)$. The first and second order derivatives of $\psi(x)$ are respectively given by

$$\dot{\psi}(x) = \frac{x-\psi(x)}{x^2}, \quad (47)$$

$$\ddot{\psi}(x) = \frac{(1+2x)\psi(x)-(x+x^2)}{x^4}. \quad (48)$$

Using the upper bound of $\psi(x)$ in (45), we see that $\dot{\psi}(x) > 0$ for $x > 0$. Thus, $\psi(x)$ is monotonically increasing in x.

In order to determine the sign of $\ddot{\psi}(x)$, we first define an auxiliary function

$$\phi(x) = e^{-1/x}\left(\psi(x) - \frac{x+x^2}{1+2x}\right). \quad (49)$$

The first order derivative of $\phi(x)$ can be expressed as

$$\dot{\phi}(x) = -\frac{2x^2 e^{-1/x}}{(1+2x)^2} < 0. \quad (50)$$

This shows that $\phi(x)$ is monotonically decreased with respect to x, so $\phi(x) < \phi(0_+) = 0$, or equivalently

$$\psi(x) < \frac{x+x^2}{1+2x}. \quad (51)$$

Substituting (51) into (48) yields $\ddot{\psi}(x) < 0$, which means that $\psi(x)$ is a concave function with respect to x. It is worth pointing out that (51) is a new upper bound of $\psi(x)$, which is tighter than that of (45) for all $x > 0$ and is tighter than that of (46) only for small positive x.

We can then prove the monotonicities of $\psi(x)$ related functions. The first order derivatives of $\theta_1(x)$, $\theta_2(x)$ and $\theta_3(x)$ are respectively given by

$$\dot{\theta}_1(x) = \frac{x-(1+x)\psi(x)}{x^3} < 0, \quad (52)$$

$$\dot{\theta}_2(x) = \frac{(x+x^2)-(1+2x)\psi(x)}{x^3} > 0, \quad (53)$$

$$\dot{\theta}_3(x) = \frac{\theta_1(bx)-\theta_2(ax)}{x}, \quad (54)$$

where the signs of (52) and (53) are determined by using (45) and (51), respectively. Thus, $\theta_1(x)$ and $\theta_2(x)$ are monotonically decreasing and increasing in x, respectively. Since $\theta_1(x)$ is monotonically decreasing in x, the sign of (54) is the same as that of $a-b$. Hence, $\theta_3(x)$ is monotonically increasing and decreasing in x for $a > b$ and $a < b$, respectively.

The function $\theta_4(x)$ defined in (18) is proportional to the slope of the line segment between fixed point $(b, \psi(b))$ and changeable point $(bx, \psi(bx))$. From the property of concave function, $\theta_4(x)$ is monotonically decreasing in x if and only if $\psi(x)$ is concave. This completes the proof of Lemma 1.

REFERENCES

[1] X. Wang, M. Chen, T. Taleb, A. Ksentini, and V. Leung, "Cache in the air: Exploiting content caching and delivery techniques for 5G systems," *IEEE Commun. Mag.*, vol. 52, no. 2, pp. 131–139, Feb. 2014.

[2] K. Shanmugam, N. Golrezaei, A. G. Dimakis, A. F. Molisch, and G. Caire, "FemtoCaching: Wireless content delivery through distributed caching helpers," *IEEE Trans. Inf. Theory*, vol. 59, no. 12, pp. 8402–8413, Dec. 2013.

[3] A. Liu and V. K. N. Lau, "Mixed-timescale precoding and cache control in cached MIMO interference network," *IEEE Trans. Signal Process.*, vol. 61, no. 24, pp. 6320–6332, Dec. 2013.

[4] A. Liu and V. Lau, "Exploiting base station caching in MIMO cellular networks: Opportunistic cooperation for video streaming," *IEEE Trans. Signal Process.*, vol. 63, no. 1, pp. 57–69, Jan. 2015.

[5] D. Liu and C. Yang, "Energy efficiency of downlink networks with caching at base stations," *IEEE J. Sel. Areas Commun.*, vol. 34, no. 4, pp. 907–922, Apr. 2016.

[6] F. Gabry, V. Bioglio, and I. Land, "On energy-efficient edge caching in heterogeneous networks," *IEEE J. Sel. Areas Commun.*, vol. 34, no. 12, pp. 3288–3298, Dec. 2016.

[7] M. Ji, G. Caire, and A. F. Molisch, "Wireless device-to-device caching networks: Basic principles and system performance," *IEEE J. Sel. Areas Commun.*, vol. 34, no. 1, pp. 176–189, Jan. 2016.

[8] M. Ji, G. Caire, and A. F. Molisch, "Fundamental limits of caching in wireless D2D networks," *IEEE Trans. Inf. Theory*, vol. 62, no. 2, pp. 849–869, Feb. 2016.

[9] M. Ji, G. Caire, and A. F. Molisch, "The throughput-outage tradeoff of wireless one-hop caching networks," *IEEE Trans. Inf. Theory*, vol. 61, no. 12, pp. 6833–6859, Dec. 2015.

[10] M. Ji, A. M. Tulino, J. Llorca, and G. Caire, "Order-optimal rate of caching and coded multicasting with random demands," *IEEE Trans. Inf. Theory*, vol. 63, no. 6, pp. 3923–3949, Jun. 2017.

[11] M. A. Maddah-Ali and U. Niesen, "Fundamental limits of caching," *IEEE Trans. Inf. Theory*, vol. 60, no. 5, pp. 2856–2867, May 2014.

[12] N. Naderializadeh, M. Ali Maddah-Ali, and A. S. Avestimehr, "Fundamental limits of cache-aided interference management," *IEEE Trans. Inf. Theory*, vol. 63, no. 5, pp. 3092–3107, May 2017.

[13] G. Paschos, E. Bastug, I. Land, G. Caire, and M. Debbah, "Wireless caching: Technical misconceptions and business barriers," *IEEE Commun. Mag.*, vol. 54, no. 8, pp. 16–22, Aug. 2016.

[14] Z. Wang and G. B. Giannakis, "A simple and general parameterization quantifying performance in fading channels," *IEEE Trans. Commun.*, vol. 51, no. 8, pp. 1389–1398, Aug. 2003.
[15] A. Alameer and A. Sezgin, "Resource cost balancing with caching in C-RAN," in *Proc. IEEE Wireless Commun. Netw. Conf. (WCNC)*, San Francisco, CA, USA, Mar. 2017, pp. 1–6.
[16] I. S. Gradshteyn and I. M. Ryzhik, *Table of Integrals, Series, and Products*, 8th ed. San Diego, CA, USA: Academic, 2014.
[17] R. Di Taranto, S. Muppirisetty, R. Raulefs, D. Slock, T. Svensson, and H. Wymeersch, "Location-aware communications for 5G networks: How location information can improve scalability, latency, and robustness of 5G," *IEEE Signal Process. Mag.*, vol. 31, no. 6, pp. 102–112, Nov. 2014.
[18] D. Slock, "Location aided wireless communications," in *Proc. 5th Int. Symp. Commun., Control Signal Process.*, Roma, Italy, May 2012, pp. 1–6.
[19] W. C. Y. Lee, "Estimate of channel capacity in Rayleigh fading environment," *IEEE Trans. Veh. Technol.*, vol. 39, no. 3, pp. 187–189, Aug. 1990.
[20] M.-S. Alouini and A. J. Goldsmith, "Capacity of Rayleigh fading channels under different adaptive transmission and diversity-combining techniques," *IEEE Trans. Veh. Technol.*, vol. 48, no. 4, pp. 1165–1181, Jul. 1999.
[21] M. Abramowitz and I. A. Stegun, *Handbook of Mathematical Functions with Formulas, Graphs, and Mathematical Tables*. New York, NY, USA: Dover, 1964.
[22] M. K. Simon and M. S. Alouini, *Digital Communication Over Fading Channels*. New York, NY, USA: Wiley-Interscience, 2005.
[23] J. H. Curtiss, "On the distribution of the quotient of two chance variables," *Ann. Math. Statist.*, vol. 12, no. 4, pp. 409–421, Dec. 1941.
[24] E. Hopf, W. Bailey, J. Whittaker, E. Landau, and J. Synge, *Mathematical Problems of Radiative Equilibrium*. Cambridge, U.K.: Cambridge Univ. Press, 1934.
[25] W. Gautschi, "Some elementary inequalities relating to the gamma and incomplete gamma function," *J. Math. Phys.*, vol. 38, nos. 1–4, pp. 77–81, Apr. 1959.

BIN JIANG (Member, IEEE) received the B.S. and Ph.D. degrees in electrical engineering from Southeast University, Nanjing, China, in 2002 and 2011, respectively. Since 2011, he has been with the National Mobile Communications Research Laboratory, Southeast University. From January to December 2017, he was a Postdoctoral Research Associate with the University of York, U.K. His research interests include signal processing and wireless communications for multiple-input–multiple-output systems. He received the Science and Technology Progress awards of the State Education Ministry of China and Jiangsu province in 2009 and 2014, respectively.

FU-CHUN ZHENG (Senior Member, IEEE) received the B.Eng. and M.Eng. degrees in radio engineering from the Harbin Institute of Technology, China, in 1985 and 1988, respectively, and the Ph.D. degree in electrical engineering from the University of Edinburgh, U.K., in 1992. From 1992 to 1995, he was a Postdoctoral Research Associate with the University of Bradford, U.K. From May 1995 to August 2007, he was with Victoria University, Melbourne, VIC, Australia, first as a Lecturer and then as an Associate Professor in mobile communications. He was a Professor (Chair) of signal processing with the University of Reading, U.K., from September 2007 to July 2016. He has been a Distinguished Adjunct Professor with Southeast University, China, since 2010. Since August 2016, he has also been with the Harbin Institute of Technology (Shenzhen), China, as a Distinguished Professor, and the University of York, U.K. He has been awarded two U.K., EPSRC Visiting Fellowships–both hosted by the University of York, U.K.: first in August 2002 and then again in August 2006. Over the past two decades, he has also carried out many government and industry sponsored research projects, in Australia, U.K., and China. He has been both a short term Visiting Fellow and a long term Visiting Research Fellow with British Telecom, U.K. His current research interests include signal processing for communications, multiple antenna systems, green communications, and ultra-dense networks. He has been an active IEEE member since 1995. From 2001 to 2004, he was an Editor of the IEEE Transactions on Wireless Communications. In 2006, he has served as the General Chair of the IEEE VTC 2006-S, Melbourne, VIC, Australia–the first ever VTC held in the southern hemisphere in VTC's history of six decades. More recently, he was the Executive TPC Chair for VTC 2016-S, Nanjing, China (the first ever VTC held in mainland China).

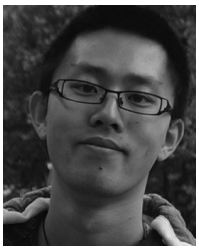

TONG PENG received the B.Eng. degree in electronics engineering from Liaocheng University, Shandong, China, in 2009, and the M.Sc. degree in communications engineering and Ph.D. degree in electronic engineering from the University of York, U.K., in 2010 and 2014, respectively. From 2014 to 2015, he was with the Centre for Studies in Telecommunications, Pontifical Catholic University, Rio de Janeiro, as a Research Associate. From 2015 to 2017, he was with the Communications Group, Department of Electronic Engineering, University of York, working on the network coded modulation for next generation wireless access networks project. He joined the Centre for Telecommunications Research, Department of Informatics, King's College London, in 2017, and was a Research Associate on the Internet of Silicon Retina Project. His research interests include space-time coding, network coding, resource allocation, and multimedia communications in the 5G IoT.

ALISTER G. BURR (Senior Member, IEEE) was born in London, U.K., in 1957. He received the B.Sc. degree in electronic engineering from the University of Southampton, U.K., in 1979, and the Ph.D. degree from the University of Bristol in 1984. From 1975 to 1985, he worked with Thorn-EMI Central Research Laboratories, London. In 1985, he joined the Department of Electronics (now Electronic Engineering) with the University of York, U.K., where he has been a Professor of communications since 2000. His research interests are in wireless communication systems, especially MIMO, cooperative systems, physical layer network coding, and iterative detection and decoding techniques. He has published around 250 papers in refereed international conferences and journals, and is the author of *Modulation and Coding for Wireless Communications* (Prentice-Hall/PHEI), and coauthor of *Wireless Physical-Layer Network Coding* (Cambridge University Press, 2018). In 1999, he was awarded a Senior Research Fellowship by the U.K., Royal Society, and in 2002, he received the J. Langham Thompson Premium from the Institution of Electrical Engineers. He has also given more than 15 invited presentations, including three keynote presentations. He was the Chair, working group 2, of a series of European COST programmes, including IC1004 Cooperative Radio Communications for Green Smart Environments, and has also served as an Associate Editor for the IEEE COMMUNICATIONS LETTERS, Workshops Chair for the IEEE ICC 2016, and the TPC Co-Chair for PIMRC 2018 and 2020.

MIKE FITCH (Member, IEEE) received the bachelor's degree in maths and physics and the Ph.D. degree in satellite communications. His previous experience is with modeling, trials and deployments of Satellite, WiMAX, 3G, and LTE systems. He is currently with BT Research and Innovation, providing technical leadership to a small research team specializing in physical and systems aspects of wireless communications. He is also involved in a number of projects on emerging wireless technologies, such as small cells, radio resource management, and 5G. In addition, he provides engineering consultancy to other parts of BT on LTE, WiFi, and other wireless topics. He is a member of IET.